JCTC Journal of Chemical Theory and Computation

Theoretical Study of the Dual Fluorescence of 4-(*N*,*N*-Dimethylamino)benzonitrile in Solution

Ignacio Fdez. Galván,* M. Elena Martín, and Manuel A. Aguilar

Química Física, Edif. José María Viguera Lobo, Universidad de Extremadura, Avda. de Elvas s/n, 06071 Badajoz, Spain

Received December 15, 2009

Abstract: We have performed high-level quantum calculations of absorption and emission properties of 4-(*N*,*N*-dimethylamino)benzonitrile (DMABN) in gas phase and in polar solvents, including the solvent effects with an explicit mean field model. Two excited states of DMABN have been found and optimized, corresponding to the two excited states assumed by the generally accepted hypotheses for the dual fluorescence of this molecule: a locally excited (LE) state and a charge transfer (CT) state. The results show that, in the gas phase, the charge transfer state is severely distorted and higher in energy than the locally excited state, while in polar solvents, it becomes almost an ideal twisted intramolecular charge transfer state (TICT) and is stabilized with respect to the locally excited state and the Franck−Condon point. The relative free energies calculated for the two excited states in solution suggest that both states are accessible from initial Franck−Condon excitation, the charge transfer state being highly favored in aqueous solution and less so in tetrahydrofuran. The results support the validity of the TICT model in this system.

1. Introduction

Since the discovery of dual fluorescence in 4-(*N*,*N*-dimethylamino)benzonitrile (DMABN), 50 years ago,[1] a great number of publications have been devoted to the investigation and explanation of its properties, as well as to similar or analogous compounds. In gas phase and in nonpolar solvents, DMABN has a single normal fluorescence band. When placed in polar solvents, it exhibits two fluorescence bands, which is an uncommon feature in fluorescence spectra. The high-energy fluorescence band corresponds to the band found in nonpolar solvents, and a new red-shifted band appears in polar solvents. Lippert et al.[1] attributed the additional band to an intramolecular charge transfer state, stabilized by the polar solvent. Grabowski et al.[2] suggested that this charge transfer state would need a twist of the dimethylamino group with respect to the phenyl ring, leading to what is known as a twisted intramolecular charge transfer (TICT) state. The participation of a TICT state is probably the most widely accepted model for the observed dual fluorescence of DMABN, but it is not the only existing explanation, a summary of other hypotheses can be found in the review by Grabowski, Rotkiewicz, and Rettig.[3] In addition to the TICT model, the participation of a planar intramolecular charge transfer state (PICT), with the dimethylamino group in the same plane as the phenyl ring, and a rehybridized intramolecular charge transfer state (RICT), with a nonlinear nitrile group, have received the most attention in recent years.

Different experimental studies[4−10] have suggested the existence of an equilibrium between the two emitting excited states, the "normal" locally excited (LE) state and the charge transfer (CT) state. Theoretical calculations, in general, support the TICT model and the interconversion between the LE and CT states as well,[8,11−18] particularly calculations that include the solvent effects, such as the work of Mennucci et al. using continuum solvation[19] or that of Minezawa and Kato with reference interaction site model (RISM) solvation.[20]

Despite the abundance of theoretical and experimental studies, the exact nature of the CT state is still under controversy. The comparison of experimental data of DMABN

* To whom correspondence should be addressed. E-mail: jellby@unex.es.

10.1021/ct9006713 © 2010 American Chemical Society
Published on Web 07/01/2010

and analogous compounds, with different geometric constraints and substituents, usually leads to various conclusions regarding the structure of the CT state. Compounds, such as 3,5-dimethyl-4-(*N*,*N*-dimethylamino)benzonitrile, where the dimethylamino group is forced to be twisted, show only the CT fluorescence band, suggesting a TICT, while other compounds where the twisting is hindered (like 6-cyano-1,2,3,4-tetrahydroquinoline, NTC6) can also present dual fluorescence, suggesting a PICT. As mentioned above, theoretical calculations tend to favor the TICT model for the DMABN molecule. For instance, the already mentioned study of Minezawa and Kato[20] ruled out the participation of a PICT state based on the calculated fluorescence energies.

In this work, we have investigated the structure and absorption and emission properties of DMABN in gas phase and in polar solvents. We considered an aprotic solvent of moderate polarity, tetrahydrofuran (THF), and a highly polar and protic solvent, water. There is experimental data on both solvents, and they will let us examine the influence that a protic solvent may have on the absorption and emission properties of DMABN. High-level quantum calculations have been performed on the ground state and two excited states (LE and CT), and the solvent effect has been included with an explicit model implementing a mean field approximation. By studying the structures and energies of the electron states presumedly implied in the dual fluorescence phenomenon, we expect to cast further light on the validity of the TICT model for this system. When appropriate, we will also compare the results obtained in this work with those of a previous study on a similar system: *N*,*N*-dimethylaniline (DMA).[21]

The rest of this paper is structured as follows. In section 2, the computational methods and details are set out; section 3 presents and discusses the results obtained from the calculations, in gas phase and in solution, and finally, section 4 contains the main conclusions we can draw from this work.

2. Methods and Details

Solvent effects on the DMABN UV/vis spectra were calculated with the ASEP/MD (Average Solvent Electrostatic Potential from Molecular Dynamics) method. This is a sequential quantum mechanics/molecular mechanics (QM/MM) method implementing the mean field approximation. It combines, alternately, a high-level quantum mechanics (QM) description of the solute with a classical molecular mechanics (MM) description of the solvent. One of its main features is the fact that the solvent effect is introduced into the solute's wave function as an average perturbation. Details of the method have been described in previous papers,[22−24] so here we will only present a brief outline.

As mentioned above, ASEP/MD is a method combining QM and MM techniques, with the particularity that full QM and MD (molecular dynamics) calculations are alternated and not simultaneous. During the MD simulations, the intramolecular geometry and charge distribution of all molecules is considered as fixed. From the resulting simulation data, the average electrostatic potential generated by the solvent on the solute (ASEP) is obtained. This potential is introduced as a perturbation into the solute's quantum mechanical Hamiltonian, and by solving the associated Schrödinger equation, one gets a new charge distribution for the solute, which is used in the next MD simulation. This iterative process is repeated until the electron distribution of the solute and the solvent structure around it are mutually equilibrated.

The ASEP/MD framework can also be used to optimize the geometry of the solute molecule.[25] At each step of the ASEP/MD procedure, the gradient and Hessian on the system's free-energy surface (including the van der Waals contribution) can be obtained, and thus, they can be used to search for stationary points on this surface by some optimization method. After each MD simulation, the solute geometry is optimized within the fixed "average" solvent structure by using the free-energy derivatives. In the next MD simulation, the new solute geometry and charge distribution are used. This approach allows the optimization of the solute geometry in parallel to the solvent structure.

For calculating transition energies, the iterative process is performed on the initial state of the transition (the ground state for absorption, the excited state for emission), that is, the atomic charges for the MD and the energy derivatives for the geometry optimization of the solute are calculated with the initial state's wave function. Then, with a frozen solvent model, the transition energies between the different states are obtained. It is also possible to calculate transition energies with a polarizable solvent model. In this case, once the solute and solvent structure have been optimized for the initial state of the solute, each state energy and wave function is calculated with the same solvent structure, but where the solvent molecules' charges are replaced by gas-phase charges plus a molecular polarizability, and an additional iterative polarization process is performed.[26,27] In this work, we used a nonpolarizable solvent model in all cases, as previous test calculations with a similar system and polarizable solvent did not show an important enough influence to compensate for the increased computational effort required.

With the transition energies calculated in solution (ΔE) and in gas phase (ΔE^0), the solvent shift δ can be obtained as the difference:

$$\begin{aligned}\delta &= \Delta E - \Delta E^0 \\ &= (\langle\Psi_{ex}|\hat{H}_{QM} + \hat{V}|\Psi_{ex}\rangle - \langle\Psi_g|\hat{H}_{QM} + V|\Psi_g\rangle) - \\ &\qquad (\langle\Psi^0_{ex}|\hat{H}^0_{QM}|\Psi^0_{ex}\rangle - \langle\Psi^0_g|\hat{H}^0_{QM}|\Psi^0_g\rangle) \\ &= (\langle\Psi_{ex}|\hat{H}_{QM} + \hat{V}|\Psi_{ex}\rangle - \langle\Psi^0_{ex}|\hat{H}^0_{QM}|\Psi^0_{ex}\rangle) - \\ &\qquad (\langle\Psi_g|\hat{H}_{QM} + \hat{V}|\Psi_g\rangle - \langle\Psi^0_g|\hat{H}^0_{QM}|\Psi^0_g\rangle)\end{aligned} \quad (1)$$

where the subindices ex and g denote the excited and ground state state of the transition, $\hat{H}_{QM}$ is the QM Hamiltonian of the solute at the in-solution geometry, without the solute−solvent interaction, $\hat{V}$, and $\hat{H}^0_{QM}$ is the QM Hamiltonian at the gas-phase geometry; Ψ and Ψ^0 are the wave functions optimized in solution and in gas phase, respectively. This solvent shift can be partitioned in different contributions, namely a geometry contribution δ_{geo}, an electronic distortion contribution δ_{dist}, and an electrostatic solute−solvent contribution δ_{elec}. If we introduce Ψ' as the wave function

optimized for the $\hat{H}_{QM}$ Hamiltonian (the geometry in solution, but without solute−solvent interaction)

$$\begin{aligned}
\delta &= \delta_{geo} + \delta_{dist} + \delta_{elect} \\
\delta_{geo} &= (\langle\Psi'_{ex}|\hat{H}_{QM}|\Psi'_{ex}\rangle - \langle\Psi^0_{ex}|\hat{H}^0_{QM}|\Psi^0_{ex}\rangle) - \\
&\quad (\langle\Psi'_{g}|\hat{H}_{QM}|\Psi'_{g}\rangle - \langle\Psi^0_{g}|\hat{H}^0_{QM}|\Psi^0_{g}\rangle) \\
\delta_{dist} &= (\langle\Psi_{ex}|\hat{H}_{QM}|\Psi_{ex}\rangle - \langle\Psi'_{ex}|\hat{H}_{QM}|\Psi'_{ex}\rangle) - \\
&\quad (\langle\Psi_{g}|\hat{H}_{QM}|\Psi_{g}\rangle - \langle\Psi'_{g}|\hat{H}_{QM}|\Psi'_{g}\rangle) \\
\delta_{elect} &= \langle\Psi_{ex}|\hat{V}|\Psi_{ex}\rangle - \langle\Psi_{g}|\hat{V}|\Psi_{g}\rangle
\end{aligned} \tag{2}$$

Thus, δ_{geo} is the solvent shift resulting from the change in geometry between gas phase and solution, δ_{elec} corresponds to the difference in solute−solvent interaction energy between the excited and ground states, and δ_{dist} to the difference in the wave function distortion energy. Note that the van der Waals component of the interaction energy is not included in the above expressions, since we adopt the approximation of considering it constant for all electronic states of the solute, and therefore, it vanishes when vertical transition energies are considered.

Once the different solute electronic states and the solvent structure around them have been optimized and equilibrated, the free energy differences between those states can be calculated, within the ASEP/MD framework, making use of the free energy perturbation method.[28,29] The expression we use to calculate the free energy difference between two species in equilibrium in solution, ΔG is

$$\Delta G = \Delta E + \Delta G_{int} + \Delta V \tag{3}$$

where ΔE is the difference in the internal quantum energy of the solute between the two species, ΔG_{int} is the difference in the solute−solvent interaction energy, which is calculated classicaly with the free energy perturbation method, and ΔV is a term that includes the difference in the zero point energy (ZPE) and entropic contributions of the solute. The last term, ΔV, is normally evaluated by applying the harmonic approximation to the vibrational modes of the solute in solution, and it needs the information provided by the Hessian matrix. In this work, obtaining an accurate enough Hessian matrix required too large computational resources, and we decided to approximate the results by neglecting this term. It must be noted that this ΔV term refers only to the internal nuclear degrees of freedom of the solute, free energy contributions from the solvent around the solute are properly accounted for in the ΔG_{int} term. Minezawa and Kato[20] estimated ZPE contributions to be typically lower than 1 kcal/mol.

The quantum calculations of the solute molecule were done with the complete active space self-consistent field (CASSCF) method,[30] using the 6-311G** basis set. Gas phase calculations were also done with the cc-pVTZ basis set. The active orbitals were the six π and π^* orbitals of the phenyl ring, the four π and π^* of the nitrile group, and the nonbonded orbital of the nitrogen, and 12 electrons were included in these orbitals, for a (12,11) total active space. Geometry optimizations in gas phase and in solution were performed except when noted on pure roots (the ground state, S_0, or the first excited singlet state, S_1), but transition energies were always calculated with a state-average (SA) calculation of the first 3 singlet states at the given geometry, S_0, S_1, and S_2. To obtain accurate transition energies, it is known that the inclusion of dynamic correlation in the quantum calculations is necessary, which we did with the complete active space second-order perturbation (CASPT2) method,[31,32] using the SA-CASSCF(12,11) wave functions as reference. A new IPEA (ionization potential - electron affinity) shifted zeroth-order Hamiltonian has been recently proposed for CASPT2 calculations,[33] which is supposed to reduce systematic overstabilization errors in open-shell systems (as is the case of the excited states studied here). We did all CASPT2 with the proposed IPEA shift of 0.25 E_h (CASPT2(0.25)), as well as with no IPEA shift (CASPT2(0.00)). To minimize the appearance of intruder states, an additional imaginary shift of 0.1i E_h was used. No symmetry was assumed in any case.

The MD simulations were carried out with rigid molecules; THF and water were used as solvents. Lennard-Jones parameters and solvent atomic charges were taken from the OPLS-AA (optimized potentials for liquid simulations, all atoms) force field,[34] solute atomic charges were calculated from the quantum calculations with the CHELPG (charges from electrostatic potential in a grid) method.[35] The geometry of tetrahydrofuran was optimized with the Becke's three-parameter Lee−Yang−Parr density functional (B3LYP)/6-311G**, for water the TIP3P model was employed. A total of 215 THF molecules or 800 water molecules, and the solute were included at the experimental density of the solvent. Periodic boundary conditions were applied, and spherical cutoffs were used to truncate the interatomic interactions at 12 Å; long-range interactions were calculated using the Ewald sum technique. The temperature was fixed at 298 K by using the Nosé−Hoover thermostat. A time step of 0.5 fs was used during the simulations, and each one was run for 100 ps after 25 ps equilibriation.

At each step of the ASEP/MD procedure, 500 configurations evenly distributed from the MD run were used to calculate the ASEP, and a radius of 15 bohr for THF and 12 bohr for water was used for including explicit solvent charges. Each ASEP/MD run was continued until the energies and solute geometry and charges are stabilized for at least 5 iterations; results are reported as the average of these last 5 iterations.

For in solution calculations, the ASEP/MD software[23] was used. During the ASEP/MD runs, quantum calculations (CASSCF optimizations) were performed with the Gaussian 98 package.[36] The final SA-CASSCF and CASPT2 calculations were done with Molcas 6.4.[37] All MD simulations were performed using Moldy.[38]

3. Results and Discussion

3.1. Gas Phase. The geometry of DMABN was optimized in gas phase at CASSCF(12,11)/6-311G** level. The resulting structure, similar to the case of *N*,*N*-dimethylaniline (DMA),[21] features a pyramidal amine N atom, slightly above the plane of phenyl ring, with the CH_3 groups below the plane forming a CH_3-N-CH_3 angle of 115.84°, and a

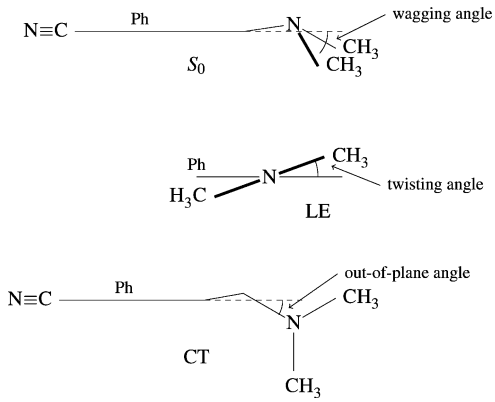

Figure 1. Scheme showing the wagging, twisting, and out-of plane angles in the ground and excited states of DMABN.

wagging angle (the angle between the CH_3-N-CH_3 plane and the phenyl ring plane) of 24.48°. This pyramidal structure and the angle values qualitatively agree with the experimental estimates[39] of 115.7° and 15°, respectively.

The first excited state, S_1, was also optimized in gas phase and, again analogously to DMA, a planar local structure on the amine N atom was obtained, with a CH_3-N-CH_3 angle of 116.91° and a twisting angle of the CH_3-N-CH_3 plane with respect to the phenyl ring of 15.53°. The experimental estimate of this angle is rather higher, 30°, but it includes significant uncertainty.[39] The bonds of the phenyl ring become longer, around 1.43 Å (they are typically 1.40 Å in the ground state), indicating a loss of aromatic character. Conversely, the bonds between the phenyl ring and the amine nitrogen and the nitrile carbon become 0.02 and 0.01 Å shorter.

Although there is no experimental evidence of emission from a CT state in gas phase, we could also optimize an excited state with high charge transfer character and perpendicular CH_3-N-CH_3 and ring planes. This state, according to the TICT model, is responsible for the dual fluorescence of DMABN observed in polar solvents. In gas phase, the torsion of the CH_3-N-CH_3 by 90° around the C−N bond is accompanied by a significant distortion of the ring, which is no longer planar (the C_4 atom moves out of the plane) and a rotation of the whole $N(CH_3)_2$ moiety, on its plane, around the C_4 atom, as displayed in Figure 1. This ring distortion agrees with the results of coupled cluster CC2 calculations.[16] The charge transfer character is reflected on the ring bond lengths, which becomes quinoidal (1.37 Å for the C_2-C_3 and C_5-C_6 bonds, 1.43 Å for the others); the phenyl−nitrogen bond is lengthened as well, from 1.37 to 1.46 Å (identical to the $N-CH_3$ bonds), while the phenyl−nitrile bond is shortened from 1.44 to 1.42 Å, which is further evidence of the decoupling between the dimethylamino and benzonitrile groups. At this distorted geometry, this state is the first excited state, and from now onward, to distinguish this state from the one in the previous paragraph, when referring to emission, we will call this state CT and the other state LE.

The absorption energies calculated at the optimized S_0 geometry are collected in Table 1. Transition energies to the first two excited states were obtained at three calculation levels (SA-CASSCF, CASPT2(0.25), and CASPT2(0.00)) and two basis sets (6-311G** and cc-pVTZ). It can be seen that SA-CASSCF values are significantly overestimated, especially for the $S_0 \rightarrow S_2$ transition, and hardly dependent on the basis set; the inclusion of dynamic correlation in CASPT2 is clearly needed to correctly reproduce even the qualitative energies of the first two absorption bands. Both CASPT2 variants, with the two triple-ζ basis sets tried, agree in providing a separation between the two absorption bands of around 0.3 eV, in good accord with the experimental values, and also in agreement with the experiments are the oscillator strengths, predicting a weak band for the almost forbidden $S_0 \rightarrow S_1$ transition and a much stronger absorption for $S_0 \rightarrow S_2$.

When comparing the two CASPT2 methods, we can observe that CASPT2(0.25) values are higher than CASPT2(0.00) ones, and all values slightly decrease when the basis set quality is improved. The same discrepancy and trend in the two methods was found in a previous study of DMA,[21] which has similar absorption properties. When the 0.25 E_h IPEA shift was proposed,[33] it was suggested that it would reduce systematic errors in open-shell systems. Our experience, however, is that CASPT2(0.00) transition energies may agree better with experiment, while CASPT2(0.25) overestimates them. We attribute this apparently poorer performance of CASPT2(0.25) to a cancellation of errors in the CASPT2(0.00) calculations: the limited basis sets and active spaces would tend to overestimate excited state energies, but this is compensated by the overstabilization of open-shell systems inherent to CASPT2(0.00). When CASPT2(0.25) is used in these cases, only the basis set and active space errors remain, and the result is an overestimation of the transition energies. In any case, for a given system and electron transition, the difference between the values of the two methods is quite constant, so that trends like solvatochromic shifts can be confidently evaluated from either of them.

In Table 2, we show the calculated band origins (energy difference between the S_0 and LE minima) and the emission energies from the two optimized excited states, LE and CT. Again, the inclusion of dynamical electron correlation improves the results, and CASPT2(0.00) gives consistently lower values for all transitions than CASPT2(0.25), while the latter overestimates the experimental data, and all values decrease with increasing basis set quality. The difference between the two transitions experimentally available is well reproduced (around 0.2 eV).

Unfortunately, there is no experimental evidence of a CT $\rightarrow S_0$ fluorescence in gas phase. The estimations in nonpolar solvents place the maximum at around 3.2 eV.[41] If this value could be transferred to the gas phase situation, it would make the CASPT2(0.00)/6-311G** result underestimated by about 0.4 eV; however, this value must be taken with caution because the above estimation is based on a very weak band that is completely buried into the more intense LE fluorescence and is, therefore, affected by a high uncertainty. Furthermore, the CC2 calculations of Köhn and Hättig,[16] where a similar geometry for the CT state was obtained, yielded also a low value for the fluorescence energy, 2.49 eV. The molecular geometries and transition energies are,

Table 1. Absorption Energies Calculated in Gas Phase (eV)[a]

	SA-CASSCF		CASPT2(0.25)		CASPT2(0.00)	
	$S_0 \rightarrow S_1$	$S_0 \rightarrow S_2$	$S_0 \rightarrow S_1$	$S_0 \rightarrow S_2$	$S_0 \rightarrow S_1$	$S_0 \rightarrow S_2$
6-311G**	4.74	6.24	4.58 (0.006)	4.90 (0.472)	4.17 (0.006)	4.46 (0.430)
cc-pVTZ	4.77	6.23	4.54 (0.006)	4.82 (0.465)	4.08 (0.005)	4.34 (0.418)
experimental[40]			4.25 (weak)	4.56 (strong)		

[a] Oscillator strength in parentheses.

Table 2. Band Origins and Fluorescence Energies Calculated in Gas Phase (eV)[a]

	SA-CASSCF			CASPT2(0.25)			CASPT2(0.00)		
	0−0	LE $\rightarrow S_0$	CT $\rightarrow S_0$	0−0	LE $\rightarrow S_0$	CT $\rightarrow S_0$	0−0	LE $\rightarrow S_0$	CT $\rightarrow S_0$
6-311G**	4.55	4.32	4.10	4.33	4.15(0.012)	3.25 (0.006)	3.91	3.75 (0.010)	2.77 (0.006)
cc-pVTZ	4.57	4.34	4.10	4.29	4.11 (0.012)	3.21 (0.006)	3.82	3.66 (0.011)	2.69 (0.006)
experimental[42]				4.00	3.76	3.2[b]			

[a] Oscillator strength in parentheses. [b] Estimation in cyclohexane.[41]

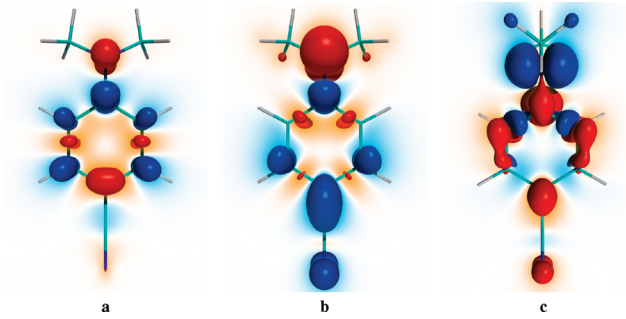

Figure 2. Electron density change in the $S_0 \rightarrow S_1$ transition (a), in the $S_0 \rightarrow S_2$ transition (b), and in the CT $\rightarrow S_0$ transition (c). Isosurfaces for a change of $0.0032e/a_0^3$: red for a decrease in density and blue for an increase. Densities calculated at SA-CASSCF/6-311G** level.

in general, in good agreement with previous ab initio calculations.[12,15,16,18,43]

To characterize the electron transitions studied in this work, we can examine differences in electron density and dipole moments. In Figure 2 we display three-dimensional maps of the electron density variation upon vertical transition, for $S_0 \rightarrow S_1$, $S_0 \rightarrow S_2$, and CT $\rightarrow S_0$ (the map for LE $\rightarrow S_0$ is quite similar, but inverted, to that of $S_0 \rightarrow S_1$). It can be observed that $S_0 \rightarrow S_1$ corresponds mainly to a local excitation in the phenyl ring, while $S_0 \rightarrow S_2$ has a marked charge transfer character, involving an important transfer of electron density from the amine N atom to the CN end of the molecule. This is also recognized from the main configuration state function (CSF) contributions in the electron states: from S_0, S_1 is well described by $\pi-\pi^*$ transitions local to the phenyl ring (particularly from the bonding to the antibonding orbitals of the C−C bonds parallel to the long axis of the molecule), S_2 corresponds mainly to a single excitation from the dimethylamino end to the rest of the molecule.[12,18] The CT $\rightarrow S_0$ transition has, as expected, a significant charge transfer character, in the opposite direction from the $S_0 \rightarrow S_2$ transition.

The dipole moments of the different states confirm the above, as seen in Table 3. In the absorption processes (S_0 geometry), the dipole moments of the S_0 and S_1 states are almost the same, confirming the "local excitation" character of the transition. The same holds for the emission from the LE state, where the dipole moments of both excited and ground state are practically identical. The dipole moment of the S_2 state, however is almost twice the as large as that of the ground state, indicative of a significant charge transfer inside the molecule. This same observation can be made in the CT geometry, where the dipole moment of the molecule is reduced to half the initial value upon emission from the CT state to the S_0 ground state.

The optimized CT state is calculated to lie 4.27 kcal/mol above the optimized LE state. If both excited states are in thermodynamic equilibrium prior to radiation emission, as suggested by several studies,[4,5,7,12] the LE state would hold more than 99.9% of the excited state population. Another important factor is the significant geometry distortion that the DMABN molecule must suffer to reach this CT state; the structure of the LE state is much more similar to the optimized S_0 geometry that the CT is. Therefore, both thermodynamic and kinetic arguments support the absence of observed emission from the CT state in gas phase.

All the above results serve to identify the geometries and electronic states that will subsequently be studied in solution. The main features are the existence of absorption processes to low-lying states of different character, and the possibility of obtaining two different optimized excited state structures, each of them of a different character as well.

3.2. Solution. The three optimized structures of DMABN (S_0, LE, and CT) were solvated in water and tetrahydrofuran, and the geometries were reoptimized with the ASEP/MD method. The geometry optimization was performed, as in gas phase, at the CASSCF(12,11)/6-311G** level; only in the case of the CT structure, it was necessary to use state averaging for the first two roots, relative weights in 1:3 proportion were used for the S_0 and CT states, respectively. Transition energies were calculated applying CASPT2 on a SA-CASSCF reference wave function, now with three states and equal weights, in all cases. We report here only CASPT2(0.00) results, the corresponding CASPT2(0.25) transitions are always around 0.4 eV higher, as observed in the gas phase.

The obtained dipole moments of the different states and the characteristic angles of the optimized structures are shown in Table 3. There are several things to be noted. The geometrical changes in the S_0 and LE structures are small in

Table 3. Characteristic Angles (Wagging Angle for S_0, Twisting Angle for LE, and out-of-Plane Angle for CT, in Degrees, see Figure 1) and Dipole Moments (at CASPT2(0.00)/6-311G** Level, in D) for DMABN

	S_0 geometry				LE geometry			CT geometry		
	wag	$\mu(S_0)$	$\mu(S_1)$	$\mu(S_2)$	twist	$\mu(S_0)$	μ(LE)	o.o.p.	$\mu(S_0)$	μ(CT)
gas	24.4	6.45	6.48	12.53	15.5	6.88	6.94	45.7	4.18	8.76
THF	23.5	7.29	7.32	13.50	7.3	8.06	8.13	31.2	6.75	17.18
water	27.8	8.19	8.11	14.64	9.8	9.41	9.59	6.9	9.64	21.26

both solvents, the overall shape of the molecule is maintained. The dipole moments of the different states are enhanced, as expected in polar solvents, but for the S_0 and LE structures the differences between states remain approximately constant. The largest variations are seen for the CT structure. Here the phenyl ring becomes increasingly planar and the out-of-plane angle progressively vanishes as the solvent polarity is increased. Simultaneously, the dipole moments of the two electron states are considerably strengthened and the difference between them becomes very large, more than 10 D. In water the molecule can be considered almost in an ideal TICT state: with a planar phenyl ring, a perpendicularly twisted dimethylamino substituent, and a very large internal charge transfer character.

Among the bond lengths, the only significant changes are a shortening of the C−N bond in the amine end, in the LE state, from gas phase to aqueous solution (0.01 Å), and in the CT state, a lengthening of the C−C bonds of the phenyl ring closer to the C≡N (0.01 Å), a shortening of those closer to the $N(CH_3)_2$ (0.02 Å), a shortening of the C−C bond between the phenyl and the nitrile (0.03 Å), and a shortening of the C−N bond in the amine end (0.04 Å). Other differences in the bond lengths are lower than 0.01 Å.

To analyze the solvent distribution around the solute molecule we refer to Figure 3, which displays the regions in space with higher concentration of oxygen atoms when the DMABN molecule is put in aqueous solution. The solvent distributions around the S_0 and LE structures show the existence of hydrogen bonding with the amine N atom in the ground state and with the phenyl ring in the excited state. However, when compared to the solvent distributions around the analogous states of DMA,[21] it is clear that the solvent structure around DMABN is significantly weaker than around DMA. This fact explains why the anomalous solvatochromic shifts of DMA in water are not observed for DMABN and supports the strong hydrogen bonds as responsible for the aforementioned anomalous behavior. This difference can be traced back to a larger negative atomic charge on the N atom in DMA: −0.64 *e* vs −0.55 *e* in DMABN.

A very strong solvent structure, however, is observed around the CT state of DMABN (Figure 3c). There are two regions of high water concentration at either side of the phenyl ring, where the water molecules orient one of their hydrogens toward the solute. Around the positions perpendicular to the $N(CH_3)_2$ plane, there is a high water concentration too, but now it is the oxygen that is oriented toward the electron-depleted nitrogen. The nitrile end forms hydrogen bonds with the solvent as well, but because of the axial symmetry, it does not induce a clear spatial orientation in the water molecules, and only the regions of high hydrogen occupancy are visible in the figure. It can be noted that the preferred hydrogen bonds are not colinear with the C≡N bond, but form an approximately tetrahedral angle, so that 3 water molecules can be simultaneously hydrogen-bonded to the nitrile.

The radial distribution functions (rdf) of water oxygens around the solute nitrogens are displayed in Figures 4 and 5. Figure 4 clearly shows the peak at 3 Å corresponding to three water molecules around the nitrile N atom of DMABN. For comparison, the rdf of DMA is also drawn, and it shows a peak for the $N(CH_3)_2$ nitrogen that is just a shoulder in DMABN; this peak corresponds to the water molecule hidrogen-bonded to the N atom thanks to its enhanced negative charge in DMA. The peak at 4.7 Å corresponds to water molecules loosely bound around the methyl groups. The rdfs for the LE state (not shown) are essentially similar to those of the S_0 state, but lacking the peak or shoulder at 3 Å for the amine nitrogen. The rdfs for the CT state are displayed in Figure 5. The peak for the nitrile nitrogen is higher, showing the increased structure of the solvent, and both rdfs have a broader peak at 4 Å, which can be attributed

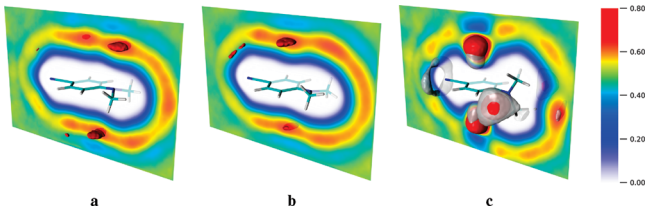

Figure 3. Occupancy maps of water oxygen atoms (considered as van der Waals spheres, as calculated by VMD[44]) around DMABN for (a) the optimized S_0 structure, (b) the optimized LE structure, and (c) the optimized CT structure. Solid red isosurfaces shown for values of 0.64 in a and b and 0.70 in c. The gray translucent surfaces in c show the occupancy of hydrogen atoms at a value of 0.42.

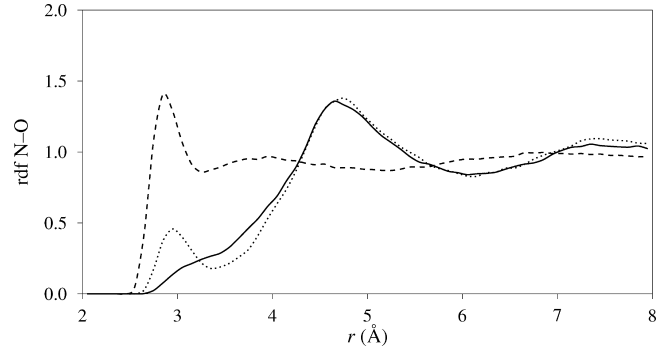

Figure 4. Radial distribution functions of water oxygen atoms around solute nitrogens for the S_0 state. Full line: $N(CH_3)_2$ nitrogen. Dashed line: C≡N nitrogen. Dotted line: DMA nitrogen (see ref 21).

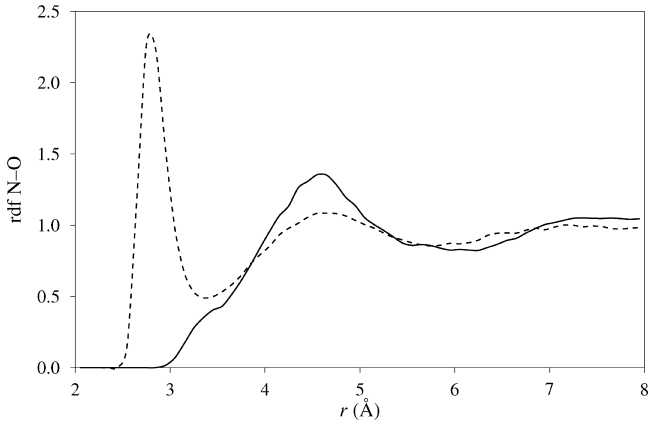

Figure 5. Radial distribution functions of water oxygen atoms around solute nitrogens for the CT state. Full line: $N(CH_3)_2$ nitrogen. Dashed line: C≡N nitrogen.

to the water molecules placed at the sides of the phenyl ring; the molecules at the sides of the $N(CH_3)_2$ group are visible as a shoulder at 3.5 Å.

Table 4 collects the calculated transition energies for the two absorption and two fluorescence bands, in gas phase and in the two studied solvents. We observe a small solvatochromic shift in the $S_0 \rightarrow S_1$ absorption band and a more significant red shift in the $S_0 \rightarrow S_2$ band, both effects being consistent with the dipole moment variations in those transitions. The energy difference between the two bands is reduced in solution, which can explain why the experimental spectra of DMABN in THF[7] and water[45] do not show any visible feature corresponding to the $S_0 \rightarrow S_1$ absorption, although in other nonpolar solvents[7] the $S_0 \rightarrow S_1$ absorption can be detected as a shoulder in the $S_0 \rightarrow S_2$ band. The calculated oscillator strengths (not shown) are very similar to the gas phase values, this supports the disappearance of the weak $S_0 \rightarrow S_1$ band into the stronger $S_0 \rightarrow S_2$ band in the absorption spectra in solution.

When comparing the current results with those obtained for DMA,[21] it can be seen that the apparent anomaly found for DMA in water (a blue shift in absorption bands, when other polar solvents induce a red shift) is not so strong in this case. There is indeed a small blue shift in the $S_0 \rightarrow S_1$ absorption, but the shift of the $S_0 \rightarrow S_2$ still occurs to the red side. This can be explained by weaker hydrogen bonds in DMABN compared to DMA as discussed above. From Table 4, it is clear that our results underestimate the red shift observed in the $S_0 \rightarrow S_2$ and LE $\rightarrow S_0$ bands when the DMABN molecule passes from gas phase to solution. For example, for the absorption band, we obtain −0.10 eV in THF and −0.15 eV in water, while the experimental values are −0.27 eV and −0.41 eV, respectively. This discrepancy can be mainly attributed to the neglect of the dispersion components of the solute−solvent interactions, as we proposed in the previous study of DMA, where we obtained a similar systematic error in solvent shifts. In DMA, the dispersion contribution was estimated in around −0.10 eV, and we can expect it to be somewhat higher, maybe up to −0.20 eV in DMABN because of the its larger size and therefore larger polarizability. The addition of this estimated error would bring the calculated solvent shift values much closer to experiment.

In the fluorescence from the LE state a small solvent effect is predicted, similarly to the $S_0 \rightarrow S_1$ absorption. The CT state is however strongly affected by the solvent, as seen in Table 3, and the corresponding fluorescence band suffers a large red shift in THF and water. Both results agree qualitatively with experimental observations,[5,7] which find that the position of the LE band is not much affected by the solvent nature, while the CT band, when present, is strongly red-shifted in polar solvents. Quantitatively, our results underestimate the red shift in the LE band, probably because of the neglect of the dispersion component, as noted above, but the shift in the fluorescence energies when passing from THF to water is correctly reproduced (−0.05 vs ±0.06 eV for LE, −0.50 vs −0.45 eV for CT). The energies for the LE fluorescence are overestimated and for the CT fluorescence are underestimated, which results in differences between the two fluorescence maxima that are too large by about 0.8 eV. This can be attributed to the apparent underestimation of the CT $\rightarrow S_0$ energy with the quantum method used, as discussed in the previous section, but also to the overstabilization of the CT state with the point-charge model used in the MD simulations, as it is known that point-charge models tend to emphasize solvent structure and charge separation. This overstabilization of the CT state further decreases the CT $\rightarrow S_0$ energy. Another reason for this problem could be the use of the same Lennard-Jones parameters for all electronic states of the solute; this can lead to unrealistic solvation for excited states when their electron distribution is significantly different from the ground state, as is the case of the CT state.

The solvatochromic shifts in the electron transitions can be partitioned as indicated it eq 2; the results are shown in Tables 5 and 6. It is evident that the electrostatic contribution δ_{elec} is dominant in both $S_0 \rightarrow S_2$ and CT $\rightarrow S_0$ transitions. The effect of the change of geometry, δ_{geo}, on the solvent shifts is small in all but the CT $\rightarrow S_0$ transition, but compared to the total δ, its relative size is more significant, showing that the effect of the solvent on the equilibrium geometries should not be neglected.

The relative free energies of the optimized LE and CT minima are given in Table 7, calculated in solution according to eq 3. In both water and THF, the CT state has a lower energy than the LE state, unlike in gas phase, where the LE state is more stable. The stabilization of the CT state is almost double in water than in THF and is dominated by the solute−solvent interaction component ΔG_{int}. These results explain qualitatively the experimental fluorescence spectra in the two solvents, with a CT band that is, in relation with the LE band, much more intense in water than in THF.[5,7]

Another quantity to consider is the relative energy of the CT state with respect to the Franck−Condon S_1 state, the results obtained are shown in Table 8 (the E_{exc} term corresponds to excitation energy $S_0 \rightarrow S_1$, calculated at the ground state geometry). In gas phase, the CT state is very close in energy to the Franck−Condon S_1 state; in water and THF the CT state lies significantly below the Franck−Condon state.

Table 4. Transition Energies (eV) Calculated in Solution at CASPT2(0.00)/6-311G** Level[a]

	absorption		fluorescence	
	$S_0 \rightarrow S_1$	$S_0 \rightarrow S_2$	LE $\rightarrow S_0$	CT $\rightarrow S_0$
gas (refs 40 and 42)	4.17 (4.25)	4.46 (4.56)	3.75 (3.76)	2.77
THF (ref 7)	4.15	4.36 (4.29)	3.74 (3.47)	2.33 (2.79)
water (refs 46 and 47)	4.21	4.31 (4.15)	3.69 (3.41−3.54)	1.83 (2.34)

[a] Experimental values in parentheses.

Table 5. Solvent Shifts and Their Components (kcal/mol) in Tetrahydrofuran Calculated at CASPT2(0.00)/6-311G** Level

	$\delta =$	$\delta_{geo} +$	$\delta_{dist} +$	δ_{elec}
$S_0 \rightarrow S_1$	−0.50	−0.14	−0.56	0.20
$S_0 \rightarrow S_2$	−2.14	−0.01	0.38	−2.59
LE $\rightarrow S_0$	−0.34	0.66	−1.04	0.04
CT $\rightarrow S_0$	−10.23	7.99	−0.36	−18.58

Table 6. Solvent Shifts and Their Components (kcal/mol) in Water Calculated at CASPT2(0.00)/6-311G** Level

	$\delta =$	$\delta_{geo} +$	$\delta_{dist} +$	δ_{elec}
$S_0 \rightarrow S_1$	0.98	0.26	0.11	0.65
$S_0 \rightarrow S_2$	−3.52	0.36	0.92	−4.77
LE $\rightarrow S_0$	−1.34	−0.12	−1.66	0.44
CT $\rightarrow S_0$	−21.65	9.44	7.40	−38.48

Table 7. Free Energy of the CT State Relative to the LE State (kcal/mol)

	$\Delta G =$	$\Delta E +$	ΔG_{int}
Gas		4.27	
THF	−5.36	4.83	−10.19
Water	−15.67	12.88	−28.55

Table 8. Free Energy of the CT State Relative to the Franck−Condon S_1 State (kcal/mol)

	$\Delta G =$	$\Delta E +$	$\Delta G_{int} -$	ΔE_{exc}
Gas	−1.67	94.55		96.21
THF	−11.46	94.23	−9.98	95.71
Water	−21.57	103.30	−27.68	97.19

The relative free energies of the different states and geometries are summarized in Figure 6. The CT state is above the LE state at both the S_0 and LE geometries in all cases. At the CT geometry, the LE state was not obtained, it is presumed to have a much higher energy. The most clear difference between the three diagrams is the great stabilization in solution of the CT state at its optimized geometry that is placed below the Franck−Condon and the optimized LE state, thus permitting the appearance of the corresponding fluorescence band.

4. Conclusions

In this work, we have shown high-level quantum calculations of absorption and emission properties of 4-(*N*,*N*-dimethylamino)benzonitrile (DMABN) in gas phase and in polar solvents: tetrahydrofuran and water. Two excited states of DMABN, with different optimum geometries, have been identified, corresponding one of them to a local excitation (LE) on the phenyl ring (S_1 at the ground state geometry) and the other to a intramolecular charge transfer (CT) from the $N(CH_3)_2$ moiety to the phenyl ring (S_2 at the ground state geometry). The CT state displays a twisted $N(CH_3)_2$ with respect to the ring, as suggested by the TICT model.

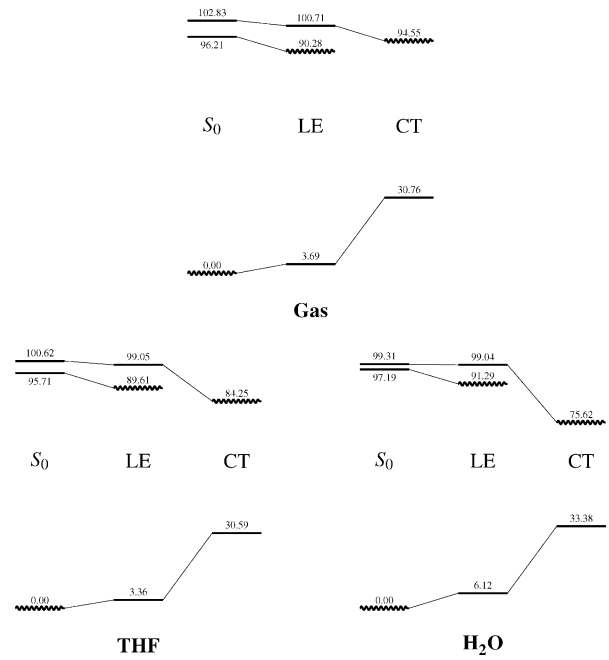

Figure 6. Relative free energies at CASPT2(0.00)//CASSCF(12,11)/6-311G** level in kcal/mol of the studied states of DMABN in gas phase and in the two solvents. The S_0, LE, and CT labels refer to the three optimized geometries obtained, and the state optimized for each geometry is marked with a wavy line.

The results for absorption show a weak S_1 band and a strong S_2 band. In solution, the S_2 band is significantly shifted to lower energies, overlapping and covering the S_1 band, which agrees with the experimental spectra.

In gas phase, the CT excited state has a higher energy than the LE state and the Franck−Condon S_1 state in absorption, and its geometry features a strongly distorted phenyl ring. This makes the CT state hardly accessible from excitation at the ground state geometry, and explains why no dual fluorescence is observed in gas phase.

In solution, the CT state acquires a more planar phenyl ring and is stabilized with respect to the LE and Franck−Condon states. In THF, all three states have a similar energy, while in water, the CT state is much more stable. The relative stabilities of the LE and CT states are in qualitative agreement with the experimental fluorescence intensities: in THF two bands of similar intensities are observed, in water the lower-energy (CT) band is much more intense.

In sum, the results of this work support the validity of the TICT model for the dual fluorescence of DMABN, since a

twisted intramolecular charge transfer state is found, it is stabilized in polar solvents, and its emission properties are in agreement with experimental observations.

Acknowledgment. This work was supported by the CTQ2008-06224 Project from the Ministerio de Educación y Ciencia of Spain and the PRI08A056 Project from the Consejería de Economía, Comercio e Innovación of the Junta de Extremadura. I.F.G. acknowledges the Junta de Extremadura and the European Social Fund for financial support.

References

(1) Lippert, E.; Lüder, W.; Moll, F.; Nägele, W.; Boos, H.; Prigge, H.; Seibold-Blankenstein, I. *Angew. Chem.* **1961**, *73*, 695–706.

(2) Rotkiewicz, K.; Grellmann, K. H.; Grabowski, Z. R. *Chem. Phys. Lett.* **1973**, *19*, 315–318.

(3) Grabowski, Z. R.; Rotkiewicz, K.; Rettig, W. *Chem. Rev.* **2003**, *103*, 3899–4032.

(4) Leinhos, U.; Kuehnle, W.; Zachariasse, K. A. *J. Phys. Chem.* **1991**, *95*, 2013–2021.

(5) Changenet, P.; Plaza, P.; Martin, M. M.; Meyer, Y. H. *J. Phys. Chem. A* **1997**, *101*, 8186–8194.

(6) Druzhinin, S. I.; Ernsting, N. P.; Kovalenko, S. A.; Pérez Lustres, L.; Senyushkina, T. A.; Zachariasse, K. A. *J. Phys. Chem. A* **2006**, *110*, 2955–2969.

(7) Galievsky, V. A.; Zachariasse, K. A. *Acta Phys. Pol., A* **2007**, *112*, S39–S56.

(8) Lee, J.-K.; Fujiwara, T.; Kofron, W. G.; Zgierski, M. Z.; Lim, E. C. *J. Chem. Phys.* **2008**, *128*, 164512.

(9) Gustavsson, T.; Coto, P. B.; Serrano-Andrés, L.; Fujiwara, T.; Lim, E. C. *J. Chem. Phys.* **2009**, *131*, 031101.

(10) Zachariasse, K. A.; Druzhinin, S. I.; Kovalenko, S. A.; Senyushkina, T. *J. Chem. Phys.* **2009**, *131*, 224313.

(11) Gorse, A.-D.; Pesquer, M. *J. Phys. Chem.* **1995**, *99*, 4039–4049.

(12) Serrano-Andrés, L.; Merchán, M.; Roos, B. O.; Lindh, R. *J. Am. Chem. Soc.* **1995**, *117*, 3189–3204.

(13) Hayashi, S.; Ando, K.; Kato, S. *J. Phys. Chem.* **1995**, *99*, 955–964.

(14) Sudholt, W.; Sobolewski, A. L.; Domcke, W. *Chem. Phys.* **1999**, *240*, 9–18.

(15) Rappoport, D.; Furche, F. *J. Am. Chem. Soc.* **2004**, *126*, 1277–1284.

(16) Köhn, A.; Hättig, C. *J. Am. Chem. Soc.* **2004**, *126*, 7399–7410.

(17) Gómez, I.; Reguero, M.; Boggio-Pasqua, M.; Robb, M. A. *J. Am. Chem. Soc.* **2005**, *127*, 7119–7129.

(18) Amatatsu, Y. *J. Phys. Chem. A* **2005**, *109*, 7225–7235.

(19) Mennucci, B.; Toniolo, A.; Tomasi, J. *J. Am. Chem. Soc.* **2000**, *122*, 10621–10630.

(20) Minezawa, N.; Kato, S. *J. Phys. Chem. A* **2005**, *109*, 5445–5453.

(21) Fdez. Galván, I.; Martín, M. E.; Muñoz Losa, A.; Aguilar, M. A. *J. Chem. Theory Comput.* **2009**, *5*, 341–349.

(22) Sánchez, M. L.; Aguilar, M. A.; Olivares del Valle, F. J. *J. Comput. Chem.* **1997**, *18*, 313–322.

(23) Fdez. Galván, I.; Sánchez, M. L.; Martín, M. E.; Olivares del Valle, F. J.; Aguilar, M. A. *Comput. Phys. Commun.* **2003**, *155*, 244–259.

(24) Aguilar, M. A.; Sánchez, M. L.; Martín, M. E.; Fdez. Galván, I. An Effective Hamiltonian Method from Simulations: ASEP/MD. In *Continuum Solvation Models in Chemical Physics*, 1st ed.; Mennucci, B., Cammi, R., Eds.; Wiley: West Sussex, England, 2007; Chapter 4.5, pp 580−592.

(25) Fdez. Galván, I.; Sánchez, M. L.; Martín, M. E.; Olivares del Valle, F. J.; Aguilar, M. A. *J. Chem. Phys.* **2003**, *118*, 255–263.

(26) Martín, M. E.; Muñoz Losa, A.; Fdez. Galván, I.; Aguilar, M. A. *J. Chem. Phys.* **2004**, *121*, 3710–3716.

(27) Muñoz Losa, A.; Fdez. Galván, I.; Aguilar, M. A.; Martín, M. E. *J. Phys. Chem. B* **2007**, *111*, 9864–9870.

(28) Zwanzig, R. W. *J. Chem. Phys.* **1954**, *22*, 1420–1426.

(29) Fdez. Galván, I.; Aguilar, M. A.; Ruiz-López, M. F. *J. Phys. Chem. B* **2005**, *109*, 23024–23030.

(30) Roos, B. O.; Taylor, P. R.; Siegbahn, P. E. M. *Chem. Phys.* **1980**, *48*, 157–173.

(31) Andersson, K.; Malmqvist, P.-Å.; Roos, B. O.; Sadlej, A. J.; Wolinski, K. *J. Phys. Chem.* **1990**, *94*, 5483–5488.

(32) Andersson, K.; Malmqvist, P.-Å.; Roos, B. O. *J. Chem. Phys.* **1992**, *96*, 1218–1226.

(33) Ghigo, G.; Roos, B. O.; Malmqvist, P.-Å. *Chem. Phys. Lett.* **2004**, *396*, 142–149.

(34) Jorgensen, W. L.; Maxwell, D. S.; Tirado-Rives, J. *J. Am. Chem. Soc.* **1996**, *118*, 11225–11236.

(35) Breneman, C. M.; Wiberg, K. B. *J. Comput. Chem.* **1990**, *11*, 361–373.

(36) Frisch, M. J.; Trucks, G. W.; Schlegel, H. B.; Scuseria, G. E.; Robb, M. A.; Cheeseman, J. R.; Zakrzewski, V. G.; Montgomery, J. A., Jr.; Stratmann, R. E.; Burant, J. C.; Dapprich, S.; Millam, J. M.; Daniels, A. D.; Kudin, K. N.; Strain, M. C.; Farkas, Ö.; Tomasi, J.; Barone, V.; Cossi, M.; Cammi, R.; Mennucci, B.; Pomelli, C. S.; Adamo, C.; Clifford, S.; Ochterski, J. W.; Petersson, G. A.; Ayala, P. Y.; Cui, Q.; Morokuma, K.; Salvador, P.; Dannenberg, J. J.; Malick, D. K.; Rabuck, A. D.; Raghavachari, K.; Foresman, J. B.; Cioslowski, J.; Ortiz, J. V.; Baboul, A. G.; Stefanov, B. B.; Liu, G.; Liashenko, A.; Piskorz, P.; Komaromi, I.; Gomperts, R.; Martin, R. L.; Fox, D. J.; Keith, T. A.; Al-Laham, M. A.; Peng, C. Y.; Nanayakkara, A.; Challacombe, M.; Gill, P. M. W.; Johnson, B.; Chen, W.; Wong, M. W.; Andrés, J. L.; González, C.; Head-Gordon, M.; Replogle, E. S.; Pople, J. A. *Gaussian 98*, revision A.11.3; Gaussian, Inc.: Pittsburgh, PA, 2001.

(37) Karlström, G.; Lindh, R.; Malmqvist, P.-Å.; Roos, B. O.; Ryde, U.; Veryazov, V.; Widmark, P.-O.; Cossi, M.; Schimmelpfennig, B.; Neogrády, P.; Seijo, L. *Comput. Mater. Sci.* **2003**, *28*, 222–239.

(38) Refson, K. *Comput. Phys. Commun.* **2000**, *126*, 310−329.

(39) Kajimoto, O.; Yokoyama, H.; Ooshima, Y.; Endo, Y. *Chem. Phys. Lett.* **1991**, *179*, 455–459.

(40) Bulliard, C.; Allan, M.; Wirtz, G.; Haselbach, E.; Zachariasse, K. A.; Detzer, N.; Grimme, S. *J. Phys. Chem. A* **1999**, *103*, 7766–7772.

(41) Schuddeboom, W.; Jonker, S. A.; Warman, J. M.; Leinhos, U.; Kuehnle, W.; Zachariasse, K. A. *J. Phys. Chem.* **1992**, *96*, 10809–10819.

(42) Lommatzsch, U.; Gerlach, A.; Lahmann, C.; Brutschy, B. *J. Phys. Chem. A* **1998**, *102*, 6421–6435.

(43) Gómez, I.; Mercier, Y.; Reguero, M. *J. Phys. Chem. A* **2006**, *110*, 11455–11461.

(44) Humphrey, W.; Dalke, A.; Schulten, K. *J. Mol. Graph.* **1996**, *14*, 33–38.

(45) Monti, S.; Marconi, G.; Manoli, F.; Bortolus, P.; Mayer, B.; Grabner, G.; Köhler, G.; Boszczyk, W.; Rotkiewicz, K. *Phys. Chem. Chem. Phys.* **2003**, *5*, 1019–1026.

(46) Figueroa, I. D.; El Baraka, M.; Quinones, E.; Rosario, O. *Anal. Chem.* **1998**, *70*, 3974–3977.

(47) Saigusa, H.; Iwase, E.; Nishimura, M. *J. Phys. Chem. A* **2003**, *107*, 4989–4998.

CT9006713